Optical Engineering

OpticalEngineering.SPIEDigitalLibrary.org

3 × 3 slot waveguide crossing based on Maxwell's fisheye lens

Seyed Hadi Badri
Mohsen Mohammadzadeh Gilarlue
Hadi Soofi
Hassan Rasooli Saghai

SPIE.

Seyed Hadi Badri, Mohsen Mohammadzadeh Gilarlue, Hadi Soofi, Hassan Rasooli Saghai, "3 × 3 slot waveguide crossing based on Maxwell's fisheye lens," *Opt. Eng.* **58**(9), 097102 (2019), doi: 10.1117/1.OE.58.9.097102.

3×3 slot waveguide crossing based on Maxwell's fisheye lens

Seyed Hadi Badri,[a,*] Mohsen Mohammadzadeh Gilarlue,[a] Hadi Soofi,[b] and Hassan Rasooli Saghai[c]
[a]Islamic Azad University, Department of Electrical Engineering, Sarab Branch, Sarab, Iran
[b]University of Tabriz, School of Engineering—Emerging Technologies, Tabriz, Iran
[c]Islamic Azad University, Department of Electrical Engineering, Tabriz Branch, Tabriz, Iran

Abstract. Intersection of two or more silicon slot waveguides is inevitable in modern optical integrated circuits based on a silicon-on-insulator platform. We design a Maxwell's fisheye lens as the crossing medium for three Si slot waveguides and numerically investigate its characteristics, such as insertion loss, cross talk, and bandwidth. For the 3×3 slot waveguide crossing, the average insertion loss of 1.2 dB and cross talk levels lower than −15.1 dB are achieved in an ultrawideband wavelength range of 415 nm covering the entire O, E, S, C, L, and U bands of optical communications. The footprint of the 3×3 silicon slot waveguide crossing presented in our paper is merely 2×2 μm^2, which is considerably smaller compared to the previously designed Si slot waveguide crossings even with fewer ports. The proposed design can be expanded to support the intersection of more slot waveguides. [DOI: 10.1117/1.OE.58.9.097102]

Keywords: slot waveguide intersection; Maxwell's fisheye lens; effective medium theory; multilayer metamaterial.

Paper 190657 received May 18, 2019; accepted for publication Aug. 13, 2019; published online Sep. 3, 2019.

1 Introduction

As the number of components on the limited space of a modern optical integrated circuit increases, crossing of waveguides becomes inevitable, which makes compact waveguide crossings indispensable components for highly dense optical and photonic integrated circuits. Therefore, various methods have been proposed in the literature to efficiently cross Si rectangular[1–5] and photonic crystal[6–10] waveguides. Si slot waveguides are key building blocks for a silicon-on-insulator (SOI) platform due to their superior characteristics, such as high light confinement and low loss. Due to these features, many devices are presented based on Si slot waveguides, such as modulators,[11,12] sensors,[13,14] light sources,[15,16] demultiplexers,[17] polarization splitters,[18] all-optical logic gates,[19] quantum optical circuits,[20] and ring resonators.[21] However, only a few designs have been presented for the crossing of Si slot waveguides. In Ref. 22, slot-to-strip mode converters followed by a multimode interference device are utilized to cross two slot waveguides resulting in an average insertion loss of ∼0.1 dB and cross talk levels of lower than −27 dB for a bandwidth of 200 nm. However, the footprint of the proposed device is considerably large, equal to 15.6×15.6 μm^2. The same method with logarithmical mode converters is also studied.[23] In a bandwidth of 200 nm, the average insertion loss is about 0.2 dB and the cross talk is lower than −33 dB. Nevertheless, the footprint of 20.8×20.8 μm^2 is the drawback of the proposed device again, which makes it incompatible for highly dense integrated circuits. The transmission efficiency can also be improved by filling up the crossing slots locally with an insertion loss of ∼1.1 dB.[24] Vertical coupling is another method presented to reduce the radiation loss in the crossing of Si slot waveguides; however, the large footprint of 13.8×0.43 μm^2[25] makes it unsuitable for compact photonic integrated circuits. It is worth noting that all the above methods only support the crossing of two waveguides with the crossing angle of 90 deg.

In this paper, we design an intersection of three Si slot waveguides based on the imaging properties of the Maxwell's fisheye (MFE) lens. Radiation of the point source on the surface of the lens is focused on the diametrically opposite point of the MFE lens. To the best of our knowledge, it is the first time that a 3×3 Si slot waveguide crossing is designed and numerically investigated. Moreover, the proposed method can be easily expanded to increase the number of intersecting waveguides by increasing the radius of the lens. The refractive index of the MFE lens is

$$n_{\text{lens}}(r) = \frac{2 \times n_{\text{edge}}}{1 + (r/R_{\text{lens}})^2}, \qquad (0 \le r \le R_{\text{lens}}), \tag{1}$$

where R_{lens} is the radius of the lens, r is the radial distance from the center of the lens, and n_{edge} is the refractive index of the lens at its edge. Recently, interesting applications have been introduced for gradient index lenses, such as MFE,[26,27] Luneburg,[28,29] and Eaton[30,31] lenses.

2 Simple Intersection of Three Slot Waveguides

In this paper, an Si slot waveguide with slot width and height of $w_s = 100$ nm and $h = 250$ nm, respectively, is considered. The width of the Si rails is $w_h = 200$ nm. Figure 1 illustrates the contour plot of the quasi-TE mode at $\lambda = 1550$ nm for the slot waveguide where silicon rails are surrounded by silica. E_x is the main electric field component, which is symmetric about the y axis and has a large discontinuity resulting in highly enhanced field in the slot. The guided mode displayed in Fig. 1 is confined in the slot by total internal reflection and consequently there are no confinement losses.[22] The electric field distribution for a simple intersection of three slot waveguides at 1550 nm is shown in

*Address all correspondence to Seyed Hadi Badri, E-mail: sh.badri@iaut.ac.ir

0091-3286/2019/$28.00 © 2019 SPIE

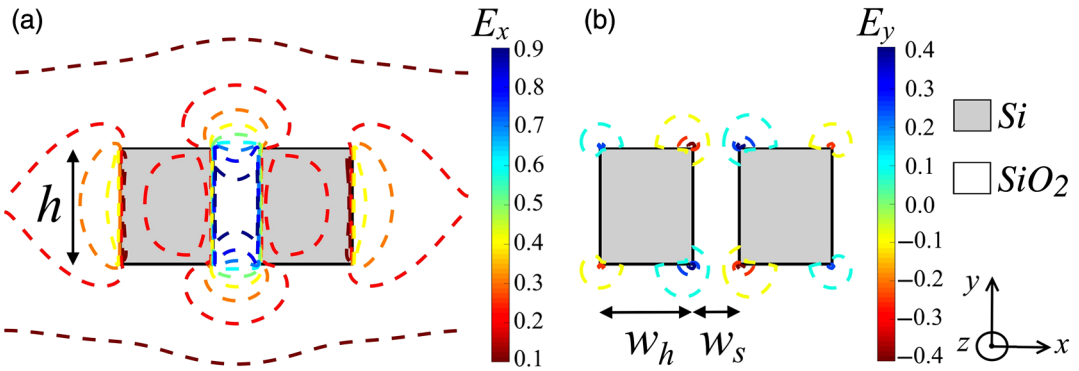

Fig. 1 The contour plot of the quasi-TE mode at $\lambda = 1550$ nm for the slot waveguide. The silicon rails are surrounded by silica.

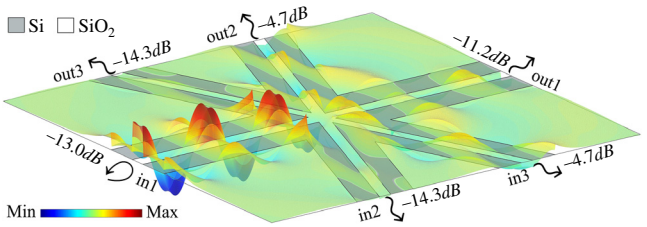

Fig. 2 The electric field distribution for a simple intersection of three slot waveguides at 1550 nm.

Fig. 2. Transmission, cross talk, and reflection values are also displayed in this figure. The diffraction at the simple intersection is considerably large, leading to substantial insertion loss of 11.2 dB, whereas the cross talk in the other ports is as high as −4.7 dB.

3 Multilayered Maxwell's Fisheye Lens Design

When the width of the layers in the multilayer structure is comparable to the wavelength of the incident light, the interference is the dominant phenomenon in determining the response of the structure. Various devices have been designed based on the interference effect in multilayer structures.[32–34] However, when the width of each layer is much smaller than the wavelength, the interference effect becomes negligible and the multilayer structure can be treated as an anisotropic metamaterial medium governed by effective medium theory.[6,35–40] We implement the MFE lens based on this concept. Due to the symmetry of the refractive index profile of the MFE lens, it can be realized by a concentric-ring multilayer structure.[6,40] When the width of each layer is much smaller than the wavelength, the multilayer structure can be regarded as an effective medium.[39] Here, silicon and silica are considered as the constituting materials of the concentric-ring multilayer structure at which Si (SiO_2) serves as the host (inclusion) material. The two components of the permittivity tensor, $\varepsilon_{\parallel}$ and $\varepsilon_{\perp}$, depend on the parallel or perpendicular arrangement of the inclusion layers with respect to the direction of the electric field and consequently have different values. In practice, the electric field is not purely TE or TM mode; therefore, the effective permittivity depends on both of these components. We simplify the design procedure by only considering $\varepsilon_{\perp}$ component[41] where the inclusion layers are perpendicular to the electric field[42]

$$\varepsilon_{\text{eff}}^{\text{TE}} = \frac{\varepsilon_{\text{host}}\varepsilon_{\text{inc}}}{\varepsilon_{\text{inc}} f_{\text{inc}} + \varepsilon_{\text{host}}(1 - f_{\text{inc}})}, \tag{2}$$

where $\varepsilon_{\text{eff}}^{\text{TE}}$ is the effective permittivity of the cell for TE mode and $\varepsilon_{\text{host}}$ and ε_{inc} are the permittivities of the host and inclusion materials, respectively. The filling factor, f_{inc}, is the fraction of the total volume occupied by the inclusion layer. In our design, the lens is divided into equal segments with a width of Λ. Afterward, the average refractive index in each layer ($\varepsilon_{\text{eff}}^{\text{TE}}$) is calculated. Subsequently, the width of the inclusion layer in the i'th layer (d_i) is calculated. To do so, Eq. (2) is rearranged to give the filling factor for the effective permittivity as

$$f_{\text{inc}} = \frac{\varepsilon_{\text{host}}(\varepsilon_{\text{inc}} - \varepsilon_{\text{eff}}^{\text{TE}})}{\varepsilon_{\text{eff}}^{\text{TE}}(\varepsilon_{\text{inc}} - \varepsilon_{\text{host}})}. \tag{3}$$

The filling factor for the i'th layer is $f_{\text{inc},i} = A_{\text{inc},i}/A_i$, where $A_{\text{inc},i} = 2\pi r_i d_i$ and $A_i = 2\pi r_i \Lambda$ are the areas of the inclusion (in the i'th layer) and the i'th layer itself, respectively. Here, r_i is the distance from the origin to the middle of the i'th layer. Therefore, d_i can be obtained by

$$d_i = \frac{\varepsilon_{\text{host}}(\varepsilon_{\text{inc}} - \varepsilon_{\text{eff}}^{\text{TE}})}{\varepsilon_{\text{eff}}^{\text{TE}}(\varepsilon_{\text{inc}} - \varepsilon_{\text{host}})}\Lambda. \tag{4}$$

The designing concept is shown in Fig. 3(a). Only a quarter of the annular rings is shown in this figure. The designed lens is illustrated in Fig. 3(b). However, the width of outer layers is <4 nm, which may not be feasible, hence, the width of the inclusion layers is limited to a more feasible value. As shown in Fig. 3(c), the inner and outer layers are limited to 35 and 18 nm, respectively. This was achieved by dividing each annular ring into annular sectors. The spacing between the center of two consecutive annular sectors was considered to be the same as the period of the structure ($\Lambda = 77.5$ nm). Then in each annular sector we placed an inclusion with the shape of an annular sector with the desired width. Similar to graded photonic crystals (GPC), the inclusions can also be in the shape of cylindrical rods. Afterward, the arc length of the inclusion sector is calculated to satisfy Eq. (3). Although, in this paper, the lens is implemented by the multilayer

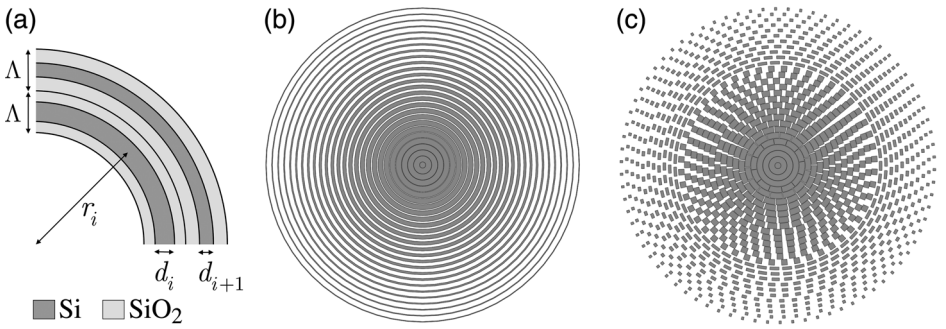

Fig. 3 (a) The designing concept for cylindrical multilayer structure. (b) Simple cylindrical multilayer structure where the outer layers are very thin. (c) The width of inclusion layers is limited by a minimum value so the arc length of inclusion layers is controlled to satisfy Eq. (3). The host material is not shown in (b) and (c).

structure, however, other methods such as varying the thickness of guiding layer and GPC can also be utilized to realize GRIN lenses.[43]

4 Results and Discussion

In this paper, a two-dimensional finite-difference time-domain (FDTD) is utilized to evaluate the performance of the proposed Si slot waveguide crossing. Such a modeling procedure is proven to be accurate for similar structures previously.[22,23,44] The built-in material models of silicon and silica of the Lumerical software are used in the simulations. A mode source is used to inject a TE mode into the simulation region where the maximum meshing step is 5 nm. The electric field distribution of the 3×3 slot waveguide crossing is shown in Fig. 4 at a wavelength of $\lambda = 1550$ nm. At this wavelength, the insertion loss is reduced from 11.2 (for the case of simple 3×3 crossing) to 1.1 dB by the help of the MFE lens. Cross talk to other ports is also reduced from -4.7 to -16.0 dB. The designed crossing has a small footprint of 2×2 μm^2. To compare the imaging quality of the designed MFE lens, the electric field intensity profiles at the input and output of the lens are compared in Fig. 5.

The scattering parameters of the 3×3 slot waveguide crossing are illustrated in Fig. 6. Since the electric field is confined in a subwavelength region in the slot waveguide, satisfying the effective medium condition requires the period of the structure to be smaller than the width of the slot. Hence, the period of the structure is chosen to be $\Lambda = 77.5$ nm. Simulations reveal that for $\Lambda > w_s$ the reflection in the interface of the slot waveguide and the MFE lens

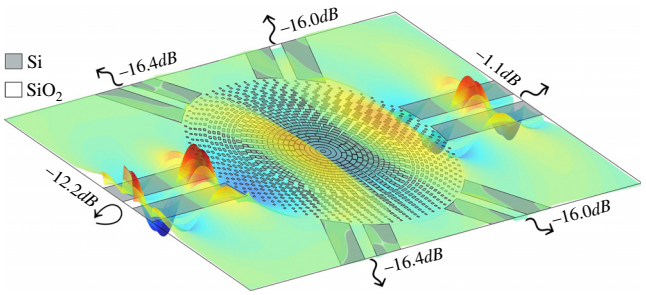

Fig. 4 The electric field distribution of the 3×3 slot waveguide crossing based on the MFE lens at a wavelength of 1550 nm.

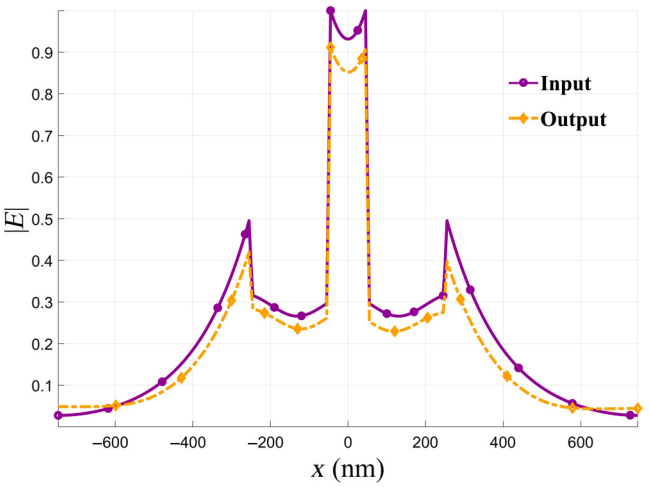

Fig. 5 Electric field intensity at the input and output of the designed 3×3 slot waveguide crossing.

structure is considerably high. In the O-band, the return loss is as high as -7 dB and, consequently, the insertion loss increases to 1.9 dB. The lowest insertion loss, 0.76 dB, is obtained at $\lambda = 1435$ nm, at which the return loss reaches its minimum value. In the C-band, the average insertion loss is 1.16 dB and the cross talk levels are lower than -16.0 dB. The return loss in this band is lower than -12 dB. For the entire O, E, S, C, L, and U bands of optical communications, the cross talk levels are lower than -15.1 dB.

Finally, it is a good practice to compare the performance characteristics of the designed lens with other Si slot waveguide crossings. The insertion loss and cross talk of previous studies[22,23,25] are better relative to the design presented in this paper. However, these designs only offer a solution for 2×2 slot waveguide crossings, whereas in this paper a 3×3 waveguide crossing is proposed. Moreover, the presented device can be simply expanded to support a higher number of waveguide crossings merely by increasing the size of the lens. Moreover, the footprint of our design is 2×2 μm^2, whereas the designs of Refs. 22, 23, and 25 have a considerably larger footprint. Other methods only offer a crossing angle of 90 deg with small deviations, whereas the crossing angle is a flexible parameter in our design. Last but not least, the design presented in this paper has the broadest bandwidth reported so far for Si slot waveguide crossings.

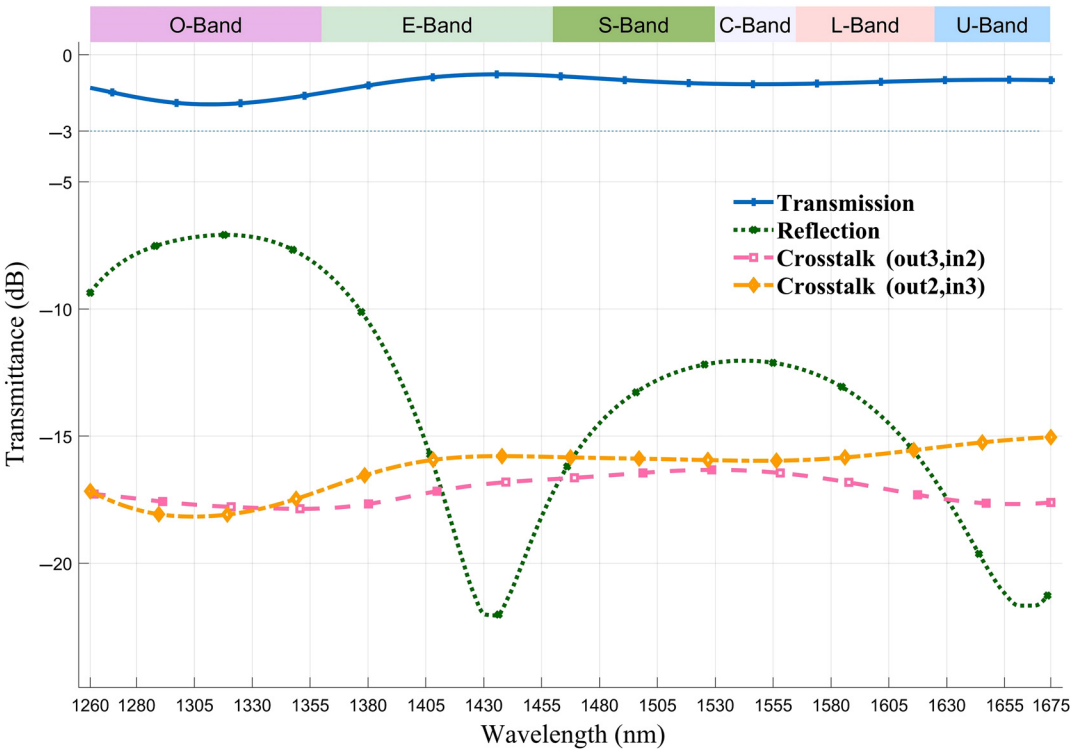

Fig. 6 The scattering parameters of the 3 × 3 slot waveguide crossing based on the MFE lens.

5 Conclusion

In this paper, a 3 × 3 Si slot waveguide crossing is proposed for the first time and numerically investigated by FDTD. We have successfully decreased the insertion loss of the simple intersection of three slot waveguides from 11.2 to 1.2 dB by utilizing the MFE lens as crossing medium. The proposed crossing is implemented by ring-based multilayer structure with a small footprint of $2 \times 2\ \mu m^2$, which is considerably small compared to the available 2 × 2 crossings. The average insertion loss is 1.2 dB and cross talk levels are below −15.1 dB in the entire O, E, S, C, L, and U bands of optical communication.

References

1. Z. Yu et al., "Inverse-designed low-loss and wideband polarization-insensitive silicon waveguide crossing," *Opt. Lett.* **44**, 77–80 (2019).
2. S. H. Badri, H. R. Saghai, and H. Soofi, "Polygonal Maxwell's fisheye lens via transformation optics as multimode waveguide crossing," *J. Opt.* **21**, 065102 (2019).
3. H.-L. Han et al., "High performance ultra-compact SOI waveguide crossing," *Opt. Express* **26**, 25602–25610 (2018).
4. W. Chang et al., "Ultracompact dual-mode waveguide crossing based on subwavelength multimode-interference couplers," *Photonics Res.* **6**, 660–665 (2018).
5. W. Chang et al., "An ultracompact multimode waveguide crossing based on subwavelength asymmetric Y-junction," *IEEE Photonics J.* **10**, 4501008 (2018).
6. M. M. Gilarlue et al., "Multilayered Maxwell's fisheye lens as waveguide crossing," *Opt. Commun.* **435**, 385–393 (2019).
7. E. Danaee, A. Geravand, and M. Danaie, "Wide-band low cross-talk photonic crystal waveguide intersections using self-collimation phenomenon," *Opt. Commun.* **431**, 216–228 (2019).
8. S. Lan and H. Ishikawa, "Broadband waveguide intersections with low cross talk in photonic crystal circuits," *Opt. Lett.* **27**, 1567–1569 (2002).
9. M. M. Gilarlue et al., "Photonic crystal waveguide intersection design based on Maxwell's fish-eye lens," *Photonics Nanostruct. Fundam. Appl.* **31**, 154–159 (2018).
10. Y. Watanabe et al., "Broadband waveguide intersection with low-crosstalk in two-dimensional photonic crystal circuits by using topology optimization," *Opt. Express* **14**, 9502–9507 (2006).
11. X. Liu et al., "Epsilon-near-zero Si slot-waveguide modulator," *ACS Photonics* **5**, 4484–4490 (2018).
12. G. Kovacevic et al., "Ultra-high-speed graphene optical modulator design based on tight field confinement in a slot waveguide," *Appl. Phys Express* **11**, 065102 (2018).
13. M. Butt, S. Khonina, and N. Kazanskiy, "Silicon on silicon dioxide slot waveguide evanescent field gas absorption sensor," *J. Mod. Opt.* **65**, 174–178 (2018).
14. C. Pan and B. Rahman, "High-sensitivity polarization-independent biochemical sensor based on silicon-on-insulator cross-slot waveguide," *IEEE J. Sel. Top. Quantum Electron.* **23**, 64–71 (2017).
15. B. Chen et al., "Investigation of germanium-loaded slot waveguides for mid-infrared third harmonic generation," *Plasmonics* **13**, 2197–2204 (2018).
16. B. Meng et al., "Tunable single-mode slot waveguide quantum cascade lasers," *Appl. Phys. Lett.* **104**, 201106 (2014).
17. T. Shoresh, N. Katanov, and D. Malka, "1 × 4 MMI visible light wavelength demultiplexer based on a GaN slot-waveguide structure," *Photonics Nanostruct. Fundam. Appl.* **30**, 45–49 (2018).
18. S. Lin, J. Hu, and K. B. Crozier, "Ultracompact, broadband slot waveguide polarization splitter," *Appl. Phys. Lett.* **98**, 151101 (2011).
19. T. Fujisawa and M. Koshiba, "All-optical logic gates based on nonlinear slot-waveguide couplers," *J. Opt. Soc. Am. B* **23**, 684–691 (2006).
20. N. Rotenberg et al., "Small slot waveguide rings for on-chip quantum optical circuits," *Opt. Express* **25**, 5397–5414 (2017).
21. W. Zhang et al., "Analysis of silicon-on-insulator slot waveguide ring resonators targeting high Q-factors," *Opt. Lett.* **40**, 5566–5569 (2015).
22. Y. Xu et al., "Design of a compact silicon-based slot-waveguide crossing," *Appl. Opt.* **52**, 3737–3744 (2013).
23. Y. Xu et al., "Design of a compact silicon-based slot-waveguide crossing composed of an orthogonal strip multimode waveguide and four logarithmical mode converters," *J. Phys. D Appl. Phys.* **46**, 455102 (2013).
24. Y. Ishizaka et al., "Three-dimensional finite-element solutions for crossing slot-waveguides with finite core-height," *J. Lightwave Technol.* **30**, 3394–3400 (2012).
25. Y. Ishizaka, K. Saitoh, and M. Koshiba, "Transmission-efficient structures of bent and crossing silicon slot waveguides," *IEEE Photonics J.* **5**, 6601809 (2013).
26. S. H. Badri and M. M. Gilarlue, "Maxwell's fisheye lens as efficient power coupler between dissimilar photonic crystal waveguides," *Optik* **185**, 566–570 (2019).
27. M. M. Gilarlue and S. H. Badri, "Photonic crystal waveguide crossing based on transformation optics," *Opt. Commun.* **450**, 308–315 (2019).

28. O. Quevedo-Teruel et al., "Glide-symmetric fully metallic Luneburg lens for 5G communications at Ka-band," *IEEE Antennas Wirel. Propag. Lett.* **17**, 1588–1592 (2018).
29. J. Li et al., "Design of a broadband metasurface Luneburg lens for full-angle operation," *IEEE Trans. Antennas Propag.* **67**, 2442–2451 (2019).
30. S. H. Badri and M. M. Gilarlue, "Low-index-contrast waveguide bend based on truncated Eaton lens implemented by graded photonic crystals," *J. Opt. Soc. Am. B* **36**, 1288–1293 (2019).
31. S. H. Badri, M. M. Gilarlue, and S. G. Gavgani, "Controlling branching angle of waveguide splitters based on GRIN lenses," arXiv:1908.05623 (2019).
32. M. F. Weber et al., "Giant birefringent optics in multilayer polymer mirrors," *Science* **287**, 2451–2456 (2000).
33. M. Yang et al., "Dielectric multilayer-based fiber optic sensor enabling simultaneous measurement of humidity and temperature," *Opt. Express* **22**, 11892–11899 (2014).
34. S. H. Badri and A. Salehi, "Realization of porous silicon multilayer bandpass filters in mid-infrared range," *Sci. Int.* **27**, 2177–2181 (2015).
35. Y. Cheng et al., "A multilayer structured acoustic cloak with homogeneous isotropic materials," *Appl. Phys. Lett.* **92**, 151913 (2008).
36. O. Kidwai, S. V. Zhukovsky, and J. Sipe, "Effective-medium approach to planar multilayer hyperbolic metamaterials: strengths and limitations," *Phys. Rev. A* **85**, 053842 (2012).
37. Q. Meng et al., "Deep subwavelength focusing of light by a trumpet hyperlens," *J. Opt.* **13**, 075102 (2011).
38. Z. Xu et al., "Concentric cylindrical metamaterials for subwavelength dark hollow light cones," *J. Opt.* **14**, 114014 (2012).
39. H. Lee et al., "Development of optical hyperlens for imaging below the diffraction limit," *Opt. Express* **15**, 15886–15891 (2007).
40. S. H. Badri, H. R. Saghai, and H. Soofi, "Polymer multimode waveguide bend based on multilayered Eaton lens," *Appl. Opt.* **58**, 5219–5224 (2019).
41. A. Sayanskiy et al., "Broadband 3-D Luneburg lenses based on metamaterials of radially diverging dielectric rods," *IEEE Antennas Wirel. Propag. Lett.* **16**, 1520–1523 (2017).
42. J. Sun, M. I. Shalaev, and N. M. Litchinitser, "Experimental demonstration of a non-resonant hyperlens in the visible spectral range," *Nat. Commun.* **6**, 7201 (2015).
43. S. H. Badri, H. R. Saghai, and H. Soofi, "Multimode waveguide crossing based on a square Maxwell's fisheye lens," *Appl. Opt.* **58**, 4647–4653 (2019).
44. R. Su et al., "Efficient transmission of crossing dielectric slot waveguides," *Opt. Express* **19**, 4756–4761 (2011).

Seyed Hadi Badri is working toward his PhD at Islamic Azad University (IAU), Azarshahr Branch, Iran. He received his BS degree in electrical engineering from IAU, Tabriz Branch, Iran, in 2004 and his MS degree from K. N. Toosi University of Technology, Iran, in 2006. He joined the Department of Electrical Engineering, IAU, Sarab Branch in 2008 as a faculty member. His current research interest field is photonic integrated devices.

Mohsen Mohammadzadeh Gilarlue received his PhD in electrical engineering from Urmia University, Urmia, Iran. He received his BS degree in electrical engineering from the University of Tabriz, Iran, in 2003 and his MS degree from the University of Tehran, Iran, in 2006. He has been a faculty member of IAU, Sarab Branch, Department of Electrical Engineering, since 2008. His research interests include transformation optics, metamaterials, metasurfaces, and innovative antenna structures.

Hadi Soofi received his PhD in optical integrated circuits from the University of Tabriz, Tabriz, Iran, in 2014. Currently, he is an assistant professor of Nanotechnology Department at the University of Tabriz. His research and teaching interests include silicon photonics, photonic-plasmonic-organic hybrid devices, and organic optoelectronics.

Hassan Rasooli Saghai received his PhD in electronics engineering from Islamic Azad University Science and Research Branch, Iran, and a postdoctoral degree in optoelectronic devices from the School of Engineering Emerging Technologies, University of Tabriz, Iran, in 2008 and 2012, respectively. He joined the Department of Electrical Engineering, Islamic Azad University, Tabriz Branch, in 2000 as a faculty member, and he is currently an associate professor. His current research interest includes quantum-based optoelectronic devices. He is the author and coauthor of more than 80 scientific international journal and conference papers and 7 text books.